Advances in Applied Mathematics and Mechanics
Adv. Appl. Math. Mech., Vol. **6**, No. 1, pp. 24-48

DOI: 10.4208/aamm.2012.m50
February 2014

Modified Ghost Fluid Method as Applied to Fluid-Plate Interaction

Liang Xu[1,2] and Tiegang Liu[2,*]

[1] *China Academy of Aerospace Aerodynamics, Beijing 100074, China*
[2] *LMIB and School of Mathematics and Systems Science, Beijing University of Aeronautics and Astronautics, Beijing 100191, China*

Received 12 December 2012; Accepted (in revised version) 17 July 2013

Available online 13 December 2013

Abstract. The modified ghost fluid method (MGFM) provides a robust and efficient interface treatment for various multi-medium flow simulations and some particular fluid-structure interaction (FSI) simulations. However, this methodology for one specific class of FSI problems, where the structure is plate, remains to be developed. This work is devoted to extending the MGFM to treat compressible fluid coupled with a thin elastic plate. In order to take into account the influence of simultaneous interaction at the interface, a fluid-plate coupling system is constructed at each time step and solved approximately to predict the interfacial states. Then, ghost fluid states and plate load can be defined by utilizing the obtained interfacial states. A type of acceleration strategy in the coupling process is presented to pursue higher efficiency. Several one-dimensional examples are used to highlight the utility of this method over loosely-coupled method and validate the acceleration techniques. Especially, this method is applied to compute the underwater explosions (UNDEX) near thin elastic plates. Evolution of strong shock impacting on the thin elastic plate and dynamic response of the plate are investigated. Numerical results disclose that this methodology for treatment of the fluid-plate coupling indeed works conveniently and accurately for different structural flexibilities and is capable of efficiently simulating the processes of UNDEX with the employment of the acceleration strategy.

AMS subject classifications: 65M06, 65N85, 74F10

Key words: Fluid-structure interaction, modified ghost fluid method, compressible flow, thin elastic plate, underwater explosions.

1 Introduction

Research on the interaction between fluid and structure, especially for the problem of strong shock impacting on the interface, has a number of important applications in mili-

*Corresponding author.
Email: xuliang@smss.buaa.edu.cn (L. Xu), liutg@buaa.edu.cn (T. G. Liu)

tary technology, homeland security and engineering. Shock waves generated by underwater explosions (UNDEX) would cause damage to vessels including hull deformation or even fracture. Generally speaking, UNDEX tests are costly and hazardous, and even may not be repeatable. Validated numerical approaches to faithfully simulate such problems are essential. The accurate numerical solution, however, may be extremely difficult to obtain due to complicated nonlinear interaction. Usually, a fluid-structure interaction (FSI) problem can be solved in a monolithic or partitioned way. The monolithic approach, where the flow and structural equations are solved simultaneously, requires a purpose-designed procedure and large computational cost. Comparatively speaking, the partitioned approach, where the flow and structural equations are solved separately, allows us to use the already existing solvers or highly developed software to treat respective media. For example, currently popular high-resolution fluid solvers, such as the discontinuous Galerkin (DG) schemes [1,2] or the (weighted) essentially non-oscillatory ((W)ENO) schemes [3,4], and high-order finite element method (FEM) can be conveniently applied in the calculation of flow and structure, respectively. The loosely-coupled method [5–9], categorized as one partitioned approach, treats the coupling conditions in an explicit manner at each time step, which means that the flow does not change while the solution of the structural equations is calculated and vice versa. This is often the method of choice, usually in most commercial software, due to its simplicity and low computational cost. But it does not enforce the equilibrium on the fluid-structure interface because the interaction is achieved by applying respective boundary conditions to the individual solver separately. Thus, the numerical instability is induced, especially when the structure is under a strong shock wave impact. On the other hand, an additional mesh deformation algorithm or remeshing technique at least in the vicinity of the interface may be required. Furthermore, it is also a challenge to conservatively map quantities from Eulerian boundary nodes to nearby Lagrangian boundary nodes, and vice versa.

Recently, a ghost fluid method (GFM) has been employed to model fluid-fluid or fluid-structure interaction in a simple and flexible way by Fedkiw et al. [10,11]. One does not need to remesh the fluid domain using this method because the moving interface is treated as an invisible internal boundary. The boundary condition is simply imposed by extrapolating specific variables from one medium to another. This treatment is classified as a partitioned approach but different from the above loosely-coupled method and, therefore, can also be regarded as a half-way-coupled method. However, it is found to be inaccurate in some situations such as high-speed jet impacting [12,13]. To overcome this problem and combine the advantages of partitioned loosely-coupled method, a modified GFM (MGFM) was proposed and developed by Liu et al. [12]. The MGFM, when used to handle fluid-fluid interaction, employs a double-shock approximate Riemann solver to determine the interface states. The predicted interface states are then used to define the fluid states in a narrow band of ghost fluid cells near the interface. The MGFM-based techniques, including its varieties like RGFM [14], have been shown to be robust and less problem-related and successfully applied to various gas-gas, gas-water coupling problems [12–16] or even solid-solid contact problems [17]. Furthermore, it has been proved

that the error estimate by the MGFM is "third-order accurate" in the vicinity of the interface for a multi-medium Riemann problem [18, 19]. Also, there have been some successful applications of this methodology to FSI problems. For example, to enable simplified elastic-plastic response, the governing equations for the solid is also Eulerian in [20–23] under assumption of a hydro-elasto-plastic material [24] for the structure subjected to a strong shock load. The interface condition, as the treatment for fluid-fluid coupling, is obtained through coupling two nonlinear characteristics from respective media. Generally, it is more common to describe the solid in a Lagrangian framework. Attempts in employing the MGFM in conjunction with various Lagrangian solid formulations have been made in recent years. For example, Liu et al. recasted the Naviers equation into a linear system and defined the interface condition through coupling a nonlinear characteristic from the fluid and a Riemann invariant from the solid [25,26]. Xie et al. combined the fluid nonlinear characteristic with the solid equation of motion to achieve the interface condition and experimented using a mass-spring model [21] or a sandwich composite structure [27–30].

However, these MGFM treatments of FSI are not suitable for a thin plate structure. The nonlinear fluid-structure coupling of strong shock impacting on a thin plate remains poorly resolved. It is the purpose of this paper to extend the MGFM to solve this FSI problem where the structure is considered as a thin elastic plate under the framework of Kirchhoff assumption. Our interest is primarily in simulating the process of strong shock wave generated by UNDEX impacting on a thin plate. The strategy in [12] is adopted to treat the explosive gas bubble-water coupling. We shall achieve a further development of the MGFM for fluid-plate coupling. The shock relationship and the equation of motion for the plate deflection are solved together to obtain internal boundary conditions. Due to our specific treatment of the interface, numerical stability in the vicinity of the fluid-plate interface can be achieved. In addition, the advantages of simplicity, low computational cost, avoidance of remeshing step and easy extension to multi-dimensions are also well inherited from the original GFM. More importantly, the nonlinear interaction between fluid and plate has been taken into account through predicting the interface states at each time step. Compared with the loosely-coupled method, the MGFM is able to provide more accurate results, especially for lower mesh density. In order to pursue higher efficiency, each fluid time step will be divided into several small time steps for the calculation of the plate. This acceleration strategy will be implemented in the MGFM.

The rest of this paper is organized as follows. In Section 2, the governing equations for both the fluid medium and plate structure are introduced. Respective solvers are also briefly described in this section. In Section 3, the MGFM is extended and applied to treat fluid-plate interaction. This is achieved mainly by constructing and solving a fluid-plate coupling system to predict the interface states. Furthermore, some acceleration techniques for the FSI simulation are presented in this section. In Section 4, the present treatment of interface condition is compared with the loosely-coupled method in several one-dimensional cases. The superiority of MGFM is confirmed through some extreme examples. In addition, the comparison of two acceleration techniques in the MGFM is

also carried out. In Section 5, an UNDEX numerical example is given to demonstrate the dynamic response of thin elastic plate subjected to shock loading. The flow fields under the different elastic moduli and rigid boundary are also simulated. Finally, conclusions are drawn in Section 6.

2 Governing equations

2.1 Fluid model

The governing equations for two-dimensional inviscid and compressible flow are Euler equations, which can be written in a conservative form as follows

$$\frac{\partial U}{\partial t}+\frac{\partial F(U)}{\partial x}+\frac{\partial G(U)}{\partial y}=0, \tag{2.1}$$

where U, $F(U)$ and $G(U)$ are the vectors of conserved variables and fluxes, given respectively by $U=[\rho,\rho u,\rho v,E]^T$, $F(U)=[\rho u,\rho u^2+p,\rho uv,(E+p)u]^T$, $G(U)=[\rho v,\rho uv,\rho v^2+p,(E+p)v]^T$. Here ρ is the density, u and v are the velocity components in the respective x- and y- directions, p is the pressure, and E is the total energy per unit volume. The total energy is written as

$$E=\rho e+\frac{1}{2}\rho(u^2+v^2), \tag{2.2}$$

where e is the internal energy per unit mass.

For closure of system (2.1), an equation of state (EOS) is required. For gases the γ-law is used as

$$p=(\gamma_g-1)\rho e, \tag{2.3}$$

where γ_g is the ratio of specific heats for gas. It is set to 1.4 for air, and 2.0 for explosive gas. Physically, the more widely accepted EOS for explosive gas is Jones-Wilkins-Lee (JWL) equation, which was derived as an analytic fit to experimental data. The simple perfect gas law is used only for computational purpose. For water the Tait EOS is used and has the form of

$$p=(\gamma_w-1)\rho e-\gamma_w B_w, \tag{2.4}$$

where $\gamma_w=7.15$ and $B_w=3.309\times10^8$Pa. The EOS above can be expressed in the following consistent form as

$$p=(\gamma-1)\rho e-\gamma B. \tag{2.5}$$

Here γ and B are set to γ_g and 0 for gas, to γ_w and B_w for water accordingly. The associated sound speed can then be expressed as $c=\sqrt{\gamma\overline{p}/\rho}$, where $\overline{p}=p+B$.

A second-order conservative scheme over a regular uniform mesh is used to discretize the Eulerian system (2.1), which is written as

$$U_{i,j}^{n+1}=U_{i,j}^n-\frac{\Delta t}{\Delta x}\left(F_{i+\frac{1}{2},j}^n-F_{i-\frac{1}{2},j}^n\right)-\frac{\Delta t}{\Delta y}\left(G_{i,j+\frac{1}{2}}^n-G_{i,j-\frac{1}{2}}^n\right), \tag{2.6}$$

where Δt, Δx and Δy are the time step size, x- and y- spatial step sizes, respectively. Numerical fluxes F^n and G^n are calculated using the second-order MUSCL approach [31] with the Harten-Lax-van Leer (HLL) approximate Riemann solver [32].

2.2 Structure model

The present work focuses on a special type of structural component, thin elastic plate, which is defined as structures possessing one dimension far smaller than the other two. The mid-plane of the plate lies along the two long dimensions of the plate, whereas the normal to the plate extends along the shorter dimension. The governing differential equation for the transverse displacement w, based on the Kirchhoff small deflection plate theory, is given by the thin-elastic-plate (or Kirchhoff) equation

$$D\nabla^2\nabla^2 w+\rho_s h\frac{\partial^2 w}{\partial t^2}=q, \tag{2.7}$$

where D is the flexural rigidity of the plate defined by

$$D=\frac{E_s h^3}{12(1-\nu^2)}.$$

In order to distinguish the x and y used in the Euler equations, we use ξ and η to denote the coordinates describing the horizontal plane of the plate. Thus, the transverse displacement w can be regarded as a function of ξ, η, t, i.e., $w=w(\xi,\eta,t)$. In the thin-elastic-plate equation, E_s, ν, h and ρ_s are constants, which respectively denote the elastic modulus (Young's modulus), Poisson's ratio, thickness and density of the plate. q is the loading function. In fluid-plate interaction q denotes the excess pressure (i.e., excluding atmospheric pressure and the weight of the plate) exerted by the fluid. ∇^2 is the two-dimensional Laplacian operator defined by

$$\nabla^2=\frac{\partial^2}{\partial\xi^2}+\frac{\partial^2}{\partial\eta^2}.$$

The boundary conditions for clamped edges are

$$w=0 \quad \text{and} \quad \frac{\partial w}{\partial n}=0, \tag{2.8}$$

and the boundary conditions for simply supported edges are

$$w=0 \quad \text{and} \quad \frac{\partial^2 w}{\partial n^2}=0. \tag{2.9}$$

Many discretization methods such as finite difference method (FDM) and finite element method (FEM) have been widely used. An advantage of FEM is the suitability for problem with complex geometries. However, the computational complexity constitutes

the main disadvantage of this technique. In this work, due to the regular geometry of the thin plate, FDM seems to be more applicable and faster to calculation. Therefore, we constructed an approximate solution by FDM. Details of discretization of Eqs. (2.7)-(2.9) can be found in Appendix. The method given in Appendix is a three-level scheme in the temporal direction. Two initial time-level conditions are then required to start the scheme. In the present applications, the initial transverse displacement w in the first two time-levels is set to zero because the plate is still initially and subsequently deformed by shock wave impacting in a late moment.

3 Fluid-plate interface treatment

The methodology for a FSI problem, in the current work, consists mainly of a compressible fluid solver, an elastic plate solver and an interface coupling technique. The existing high-order algorithms can be adopted for respective media. Therefore, often the most difficult part is to faithfully capture the effect of complex fluid-structure nonlinear interaction.

3.1 Motivation

In a MGFM-based algorithm for treating multi-fluid Euler-Euler coupling with an immiscible material interface, a narrow band of 3 to 5 grid points as ghost cells is defined in the vicinity of the material interface. At the ghost cells, ghost fluid and real fluid coexist. To define ghost fluid states for the ghost cells, a multi-medium Riemann problem is constructed along the normal direction of material interface. An approximate Riemann problem solver with a doubled-shock structure [33] is employed to predict the interface states. Finally the ghost fluid states are obtained by using the predicted interface states. More can be found in [12]. Thus, we can employ our favorite single medium numerical solver to solve for each medium covering both the real fluid nodes and ghost fluid nodes next to the interface. By combining the solution for each medium according to the new interface location, we then obtain the overall solution valid for the whole computational domain at the new time step.

As for the FSI where one Eulerian fluid is coupled with one Lagrangian solid, the mutual interaction often leads to highly nonlinear behavior and the development of robust and efficient solution techniques for such problems presents one of the great challenges in computational mechanics. Usually, most commercial software is known to adopt the "loosely-coupled" strategy by solving the flow equations and the structural equations in a sequential and staggered way. As shown in Fig. 1, the fluid is usually solved first with the structure assumed rigid, and then the structure is solved via imposing the force boundary conditions, which is obtained from the fluid solver, on the structure surface. The interface location obtained from the solid solver serves as the new boundary for the fluid solver in the next round of computation. It is obvious that this treatment does not

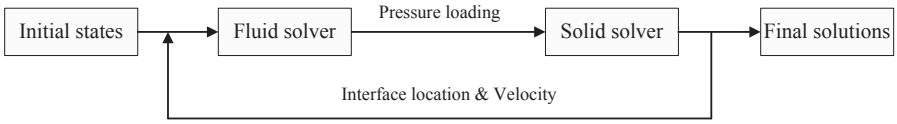

Figure 1: Diagram of coupling between fluid and solid solvers using loosely-coupled method.

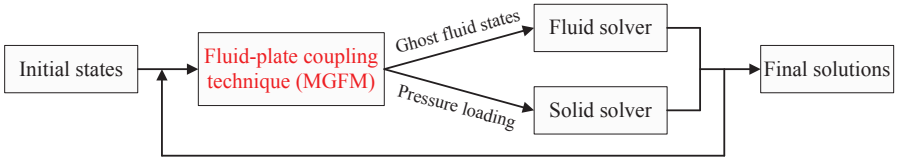

Figure 2: Diagram of coupling between fluid and solid solvers using MGFM.

truly reflect the complex interaction and impose the equilibrium conditions at the interface. As a consequence, this explicit coupling is only suitable for weak interactions like aeroelastic simulation with a rather stiff structure. Furthermore, mesh regeneration or special technique of treating irregular grid cells for the fluid solver seems essential at least in the vicinity of the interface. Motivated by the existing MGFM applied to multi-medium Riemann problem, we shall extend it to the computation for coupling between the fluid and the elastic plate. Such treatment is classified as a partitioned algorithm, but significantly alleviates the shortcomings of the loosely-coupled method via predicting the interface states to define the ghost fluid states and the pressure loading. The current implementation is depicted in Fig. 2. In addition, this method is also suitable for a fixed Eulerian mesh construction, avoiding any mesh deformation or remeshing step.

3.2 Fluid-plate coupling system

When the MGFM is applied to treat the fluid-plate coupling where the plate is described using (2.7), it is not convenient and easy to construct a fluid-plate Riemann problem at the interface. But we can utilize the original MGFM implementation by replacing the multi-medium Riemann problem with a fluid-plate coupling system. We assume that the fluid is located on the left side of the interface (thin plate). For one-dimensional case, the fluid-plate coupling system can be written as

$$\begin{cases} \dfrac{\partial U}{\partial t}+\dfrac{\partial F(U)}{\partial x}=0, & \text{with } U|_{t=0}=U_l \text{ for } x<x_0, \\ D\nabla^2\nabla^2 w+\rho_s h\dfrac{\partial^2 w}{\partial t^2}=q, & \text{with } w|_{t=0}=w_0 \text{ for } x=x_0, \end{cases} \tag{3.1}$$

where $U=[\rho,\rho u,E]^T$, $F(U)=[\rho u,\rho u^2+p,(E+p)u]^T$. Here, u is the normal velocity. U_l is the constant flow status on the left-hand medium. x_0 is the initial interfacial location, and it also represents the initial location of the thin plate in the normal direction. In general, the transverse displacement w_0 is initially zero for a plate bending problem. Once the "diaphragm" separating the fluid and plate is removed, the interface moves with the plate transverse velocity and the transverse displacement changes.

When employed to solve fluid-plate coupling system (3.1), the MGFM-based techniques require essentially solving one pure medium Riemann problem (called GFM Riemann problem) in the fluid medium with associated one-sided ghost fluid at each time step. The GFM Riemann problem can be expressed as

$$\frac{\partial U}{\partial t}+\frac{\partial F(U)}{\partial x}=0,\quad U|_{t=0}=\begin{cases} U_l, & x<x_0,\\ U_r^*, & x>x_0.\end{cases} \tag{3.2}$$

It solves from the grid node 1 on the left end to the ghost node next to the interface. Hereafter, "$*$" indicates the ghost fluid (status). On the other hand, the thin-elastic-plate equation should be solved simultaneously. This equation, therefore, can be written as

$$D\nabla^2\nabla^2 w+\rho_s h\frac{\partial^2 w}{\partial t^2}=q^*. \tag{3.3}$$

Here, q^* should be interpreted as $q^*=p^*-p_0$ with predicted pressure loading p^*. p_0 can be taken as the atmospheric pressure or zero, as required.

3.3 MGFM for interface treatment

In order to ensure the equilibrium on the fluid-plate interface within one time step, the ghost fluid status U_r^* and pressure loading p^* should be faithfully defined in advance. In fact, there is one nonlinear characteristic from the fluid medium intersecting with the interface. The characteristic equation in association with the Eulerian system can be written as

$$\frac{dp_I}{dt}+\rho_{IL}c_{IL}\frac{du_I}{dt}=0\quad\text{along}\quad\frac{dx}{dt}=u_I+c_{IL}. \tag{3.4}$$

The subscript I refers to the interface and IL denotes the left side of the interface. On the other hand, the discrete analogue of (2.7) is given by

$$D\nabla_h^2\nabla_h^2 w+\rho_s h\frac{u^{n+1}-u^n}{\Delta t}=p_I-p_0, \tag{3.5}$$

where $\nabla_h^2\nabla_h^2 w$ denotes the discrete form in space (see Appendix), $u=\partial w/\partial t$ denotes the plate transverse nodal velocity. Following the treatment used in [12] for (3.4) together with the discrete equation (3.5), we solve a coupled system

$$\begin{cases} \dfrac{p_I-p_l}{W_l}+(u_I-u_l)=0,\quad W_l=\rho_l c_l\sqrt{1+\dfrac{\gamma_l+1}{2\gamma_l}\dfrac{p_I-p_l}{p_l+B_l}},\\ \dfrac{p_I-(p_0+D\nabla_h^2\nabla_h^2 w)}{\rho_s h/\Delta t}-(u_I-u_I^n)=0, \end{cases} \tag{3.6}$$

to predict the fluid-plate interface states. In the above system, the EOS for fluid is based on (2.5). w_I^n and u_I^n in (3.6) can be obviously chosen as the plate transverse nodal displacement and velocity at time $t=t^n$. We also need to determine the fluid state U_l, i.e.,

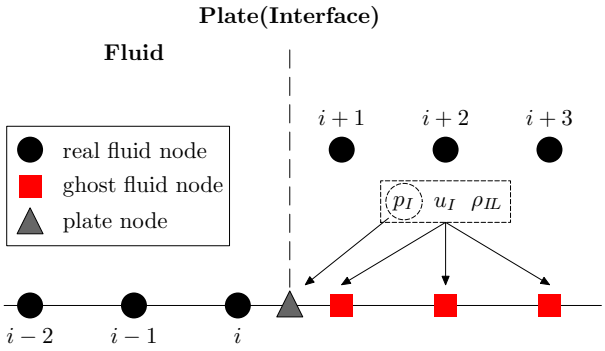

Figure 3: 1D schematic diagram for treating a fluid-plate interaction in the MGFM.

(ρ_l,u_l,p_l,c_l). Assuming that the plate is located next to node i at time $t=t^n$, U_l can be obtained via interpolation along the characteristic lines $dx/dt=u_I+c_{IL}$ tracing back from the interface into the fluid medium. Alternatively, U_l can simply be taken as U_{i-1}. Then, the interface states can be obtained by solving (3.6) using iterative method.

After the predicted pressure and velocity at the interface are solved, the predicted density can be obtained by utilizing the shock relationship. Then, as depicted in Fig. 3, we could define the ghost fluid states and the plate load: for the fluid, the predicted pressure p_I, velocity u_I and density ρ_{IL} are defined as the ghost fluid states; for the plate, only the result of p_I-p_0 is defined as the load. It is worth remarking that the computational fluid domain should include at least two nodes across the interface. These nodes are served as the ghost fluid nodes, as $i+1$, $i+2$ and $i+3$ shown in Fig. 3.

The methodology in the current work does not require an interface capturing technique, such as the level set technique [34] or the front tracking technique [35], which is usually combined with the MGFM-based algorithm to obtain a moving "sharp" interface for multi-medium problems. For the fluid-plate interaction, the interface location is given by the solution of thin-elastic-plate equation (2.7). As shown in Fig. 3, there are respective mesh systems for Eulerian and Lagrangian coordinates, where the fixed Cartesian Eulerian fluid cells are distributed across the thin plate (interface) and the mesh nodes may not necessarily locate at the plate. The new interface location at $t=t^{n+1}$ can be expressed as

$$x_I^{n+1}=x_0+w|_{t=t^n}. \tag{3.7}$$

For each time iteration, the interface location is used to distinguish real cells within the fluid domain and ghost cells on the other side of interface.

In the two-dimensional computations, we need to choose two corresponding nodes along the normal direction: one is adjacent to the plate in the fluid region; the other is a plate node, as nodes A and B marked in Fig. 4(a). The normal velocity u_N^A, as the u_l in (3.6), is obtained via projecting fluid x- and y- velocity components into the normal direction of the plate. The nodal velocity u_I^n is taken as the one of last time step. After solving the system (3.6) we can define the ghost fluid stats and the plate load. The x- and

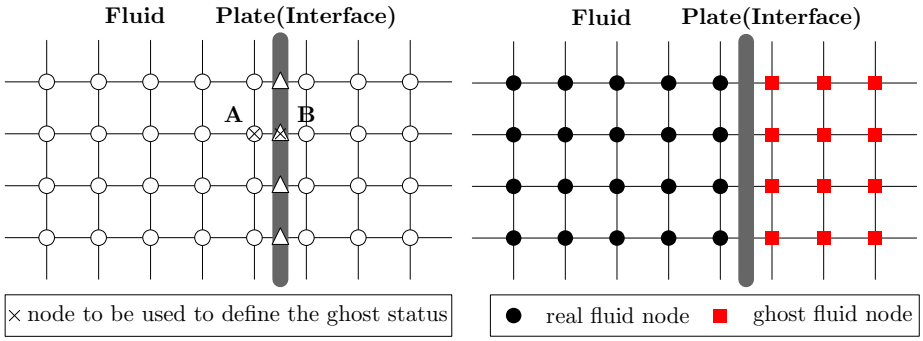

(a) Construction of the coupled system (b) Definition of the ghost fluid states

Figure 4: Illustration of the MGFM treatment for the fluid-plate interface.

y- ghost fluid velocity can be calculated comprising the ghost normal velocity component and the real tangential velocity component. See Fig. 4(b). It should be pointed out that an interpolation procedure is usually required to obtain the respective states at point A or B during the construction of the fluid-plate coupled system to predict the interface state. More specifically, to obtain and define the ghost fluid state for point A, point B on the plate may not be a Lagrangian mesh point. Interpolation on the plate is applied to obtain the plate state at point B and vice versa. It should be further noted that a narrow band of ghost fluid cells are defined on the other side of the interface. Other fluid cells beyond the ghost fluid region are not solved for, but are used simply to reserve the space to allow bending deformation of the plate without the need to remesh the fixed fluid grid. When the plate deforms, the ghost fluid cells in the vicinity of the plate may become real fluid cells.

Here we briefly summarize the general procedure of fluid-plate coupling using the MGFM algorithm:

Step 1 Predict the fluid-plate interface states by solving coupled equations (3.6), and then use the solutions to define ghost fluid states and pressure loading.

Step 2 Choose a suitable high-order single medium scheme to solve for each medium. In that way the solution in all the media is advanced to the new time step.

Step 3 Obtain the final solution over whole computation domain according to the new interface location (3.7), and then update the new time step size and proceed to the next time step.

3.4 Acceleration of the coupling process

The MGFM utilizes the information in the vicinity of the interface at $t = t^n$ to predict the embedded boundary conditions, and then defines the ghost fluid states and pressure loading. In accordance with certain coupling time step Δt, both media are simultaneously advanced to $t = t^{n+1}$, as shown in Fig. 5(a). To ensure computational stability, the CFL

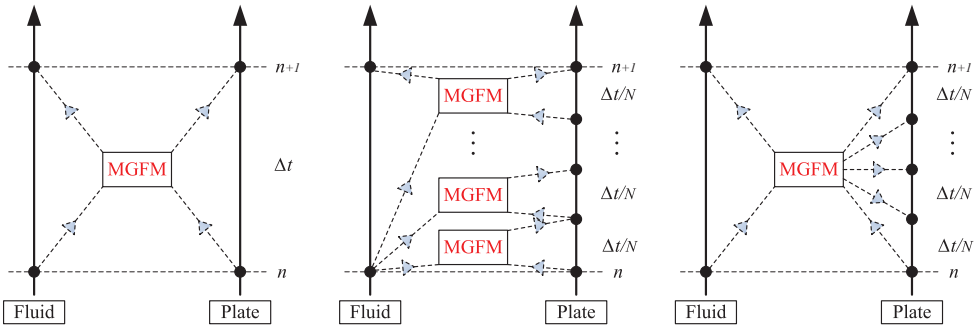

(a) No acceleration technique (b) Acceleration technique 1 (c) Acceleration technique 2

Figure 5: Illustration and comparison of several acceleration techniques.

condition for the fluid medium is set as

$$\Delta t_f = \mathrm{CFL}\frac{\min(\Delta x,\Delta y)}{\max\limits_{i,j}(|u_{i,j}|+|v_{i,j}|+c_{i,j})}, \tag{3.8}$$

where $u_{i,j}$, $v_{i,j}$ and $c_{i,j}$ are the x- and y- velocity components and sound speed at each grid point, respectively. The time step size for the plate calculations can be taken as

$$\Delta t_s \leq \frac{1}{2}\sqrt{\frac{\rho_s h}{D}}\left(\frac{1}{\Delta\xi^2}+\frac{1}{\Delta\eta^2}\right)^{-1}, \tag{3.9}$$

through the stability analysis of scheme (A.2) using the Fourier method. The final time step size, which must satisfy the stability restrictions of both fluid and structural field, can be taken as

$$\Delta t = \min(\Delta t_f,\Delta t_s). \tag{3.10}$$

The time step size for computing the plate is usually much smaller than that for the fluid, i.e., $\Delta t_s \ll \Delta t_f$, say, for a large elastic modulus or nearly same order of both fluid and solid mesh sizes. Therefore in such applications, the coupling time step Δt will be dictated by the time step Δt_s, rather than the time step Δt_f. If we typically take this time step as the coupling time step, the computational cost is often too high. In order to pursue higher efficiency, we can change the mesh size in the structural domain, i.e., to increase $\Delta\xi$ and $\Delta\eta$ in (3.9). This is a natural and reasonable choice in most if not all small deformation cases, because the structural field, compared with flow field, usually does not require a very fine spatial resolution. But the mesh size of the plate can not be increased unlimitedly. Excessive increase will inevitably lead to distortion of the results. To further pursue higher efficiency and ensure strict synchronization between the fluid and structural domains, other strategies based on structural substep are designed as follows.

In each fluid time step, we choose $\Delta t = \Delta t_f$ as the final time step. That time step is divided into several small time steps for the calculation of the plate, i.e., $\Delta t_s = \Delta t_f/N$.

Δt_s is so designed as to satisfy the stability requirement of (3.9). N substeps of the plate computations can contribute to save the overall simulation CPU time because in that case the flow field will be advanced fewer times. The structural nodal load can be defined as follows. We predict the structural nodal load for each substep $\Delta t/N$ using the MGFM. After the solid solution at $t=t^n+\Delta t/N$ is obtained, we repeat the above process for the next sub-time step. This acceleration technique is illustrated in Fig. 5(b). Alternatively, the nodal load of plate can simply be regarded as constant in each substep, as shown in Fig. 5(c). These two techniques are respectively called "Technique 1" and "Technique 2" in the following sections. The results are insensitive to the time step sizes as long as stability is guaranteed.

It is worth mentioning that the prediction of interfacial states using the MGFM is not time-consuming as part of numerical procedures, because the interface here is a lower dimensional grid and the number of the points required to predict is therefore limited. In view of this fact, it is easy to see that the speedup ratio t_N/t_Y using the above acceleration strategies is between 1 and N, where t_N represents the overall computation time for one numerical example without any acceleration technique, and t_Y represents the overall time with certain acceleration technique. The so-called speedup ratio is close to 1 if the computing time for structure is dominant compared to fluid calculation, and close to N if the computing time for flow field is dominant, such as in this work. Certainly, we are not free to choose the number N at our will. The value of N should be appropriate and problem-related. On one hand, it should make the solid calculation satisfy the stability condition (3.9) and therefore too small value is not suitable. On the other hand, the distortion of the numerical results will be more and more evident with the increase of N.

4 Method validations and comparisons

Now we make some validations for the MGFM by several one-dimensional fluid-plate interaction problems. For comparison, we also solve some of these test problems using the loosely-coupled method. Let us consider an infinitely long plate simply supported along two opposite edges. The center of the plate is assumed to be the right boundary of one-dimensional fluid region. The nodal load of this point, obtained in each time step, is constantly extrapolated to other grid points. So the plate is only subjected to a uniformly distributed load, and its transverse loading q is just a function of time t. In this situation, the two-dimensional solid equation (2.7) can be simplified as

$$D\frac{\partial^4 w}{\partial \xi^4}+\rho_s h\frac{\partial^2 w}{\partial t^2}=q. \tag{4.1}$$

Actually, (4.1) is similar to the dynamic Euler-Bernoulli beam equation [36]. Fig. 6 shows a simple illustration of this problem. For convenience the fluid variables are scaled as

$$\overline{x}=\frac{x}{l_0},\quad \overline{u}=\frac{u}{u_0},\quad \overline{\rho}=\frac{\rho}{\rho_0},\quad \overline{p}=\frac{p}{\rho_0 u_0^2},\quad \overline{t}=\frac{t}{l_0/u_0},\quad \overline{E}=\frac{E}{\rho_0 u_0^2}, \tag{4.2}$$

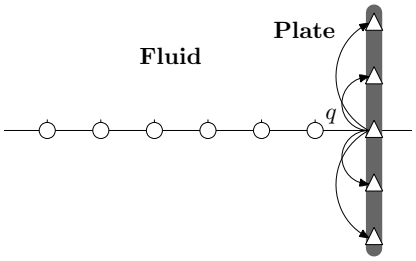

Figure 6: Sketch of 1D fluid-plate coupling.

with l_0=1.0m, u_0=10.0m/s, ρ_0=1.0×10^3kg/m^3 the reference length,velocity and density, respectively. This results in the same equations for the non-dimensional parameters as for the dimensional parameters, except that all variables have an overbar. The additional plate variables, similarly, are scaled as

$$\overline{\xi}=\frac{\xi}{l_0},\quad \overline{w}=\frac{w}{l_0},\quad \overline{h}=\frac{h}{l_0},\quad \overline{\rho_s}=\frac{\rho_s}{\rho_0},\quad \overline{E_s}=\frac{E_s}{\rho_0 u_0^2}. \tag{4.3}$$

The equation has the same form as (4.1). For notation purposes the bars are dropped in the remainder of this subsection.

The material of the plate, except for special explanation, is chosen to be aluminum, for which some non-dimensional parameters, such as elastic modulus of 7.1×10^5, density of 2.7, Poisson's ratio of 0.33, side length of 10.0 and thickness of 0.1 are assumed. Since this problem has no exact analytical solution and the solutions by the MGFM and the loosely-coupled method are nearly identical as the mesh size tends to zero, we therefore take the result obtained with a fine mesh of $\Delta x=1.0\times10^{-4}$ in the fluid domain and $\Delta\xi=0.1$ in the solid domain as the reference solution. In the following cases, we regard this as the "exact" solution and use it to compare with the "numerical" solutions obtained in coarse meshes. Note that the right boundary of the fluid domain changes with time due to fluid-plate interaction. The initial non-dimensional flow conditions and other computational parameter settings can be found in Table 1.

Table 1: Initial data and parameters.

	Fluid medium	Initial conditions				Computation time
		ρ_l	u_l	p_l	x_0	
Case 4.1	Air	0.2	1.0×10^3	1.0	0.3	1.0×10^{-3}
Case 4.2	Water	1.0	1.0×10^2	1.0	0.4	1.0×10^{-3}
Case 4.3	Air	0.2	1.0×10^4	1.0	0.3	4.27×10^{-5}
Case 4.4	Air	0.2	1.0×10^4	1.0	0.3	6.4×10^{-5}

Case 4.1 (Grid convergence)**.** This is a problem where a shock wave is generated in the air medium. In this case, we give a comparison between the MGFM and the loosely-coupled

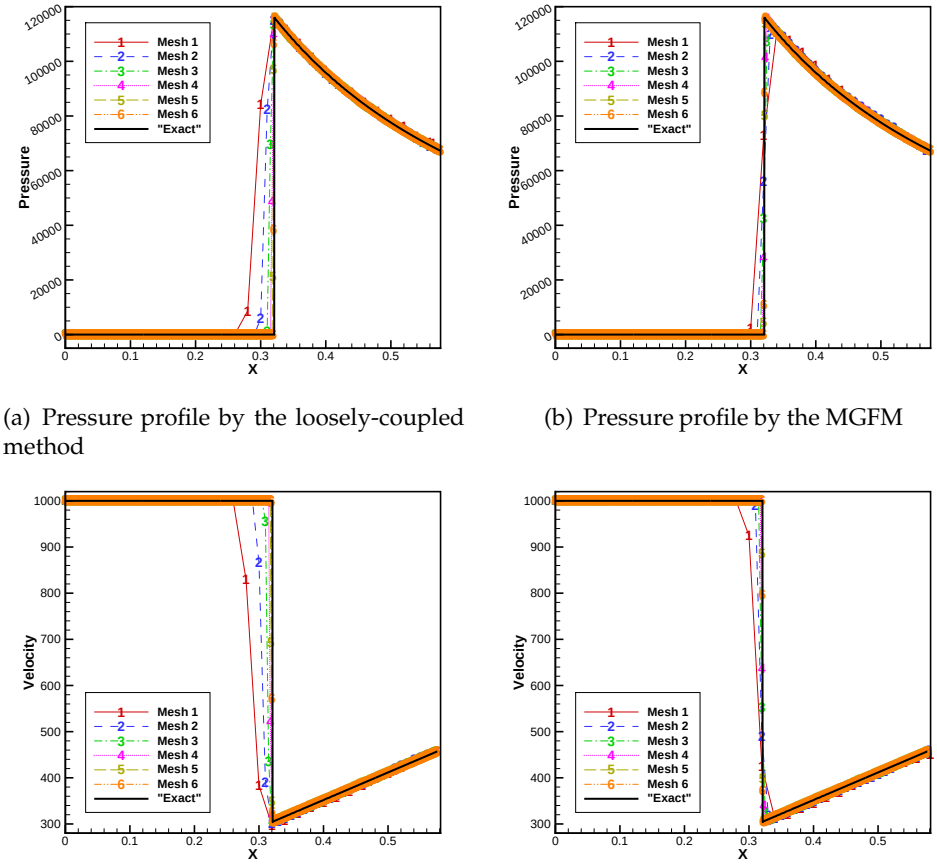

(a) Pressure profile by the loosely-coupled method

(b) Pressure profile by the MGFM

(c) Velocity profile by the loosely-coupled method

(d) Velocity profile by the MGFM

Figure 7: Case 4.1: Comparison of different mesh densities at $t=1.0\times10^{-3}$.

method with different grid numbers in the fluid domain. The solid domain is discretised by equally spaced cells of width $\Delta\xi=0.5$. Six fluid meshes are examined: Mesh 1: $\Delta x=2.0\times10^{-2}$, Mesh 2: $\Delta x=1.0\times10^{-2}$, Mesh 3: $\Delta x=5.0\times10^{-3}$, Mesh 4: $\Delta x=2.5\times10^{-3}$, Mesh 5: $\Delta x=1.25\times10^{-3}$, Mesh 6: $\Delta x=6.25\times10^{-4}$. The MGFM, on a same mesh, is better than the loosely-coupled method for capturing the location of the shock front, as shown in Figs. 7(a)-7(d). The pressure and velocity profiles also show that the MGFM on Mesh 2 affords a comparable result to the "exact" solution, but similar result for the loosely-coupled method can only be observed on a finer mesh. It is obvious that the results from the MGFM and from the loosely-coupled method have no essential difference with sufficiently fine mesh. However, fewer grids can achieve satisfactory results in the MGFM, and this can not be carried out in the loosely-coupled method.

Case 4.2 (Water-plate interaction on a coarse mesh)**.** As shown in Case 4.1, the MGFM is more capable of treating the problem with fewer grids. In the following, we solve a water-

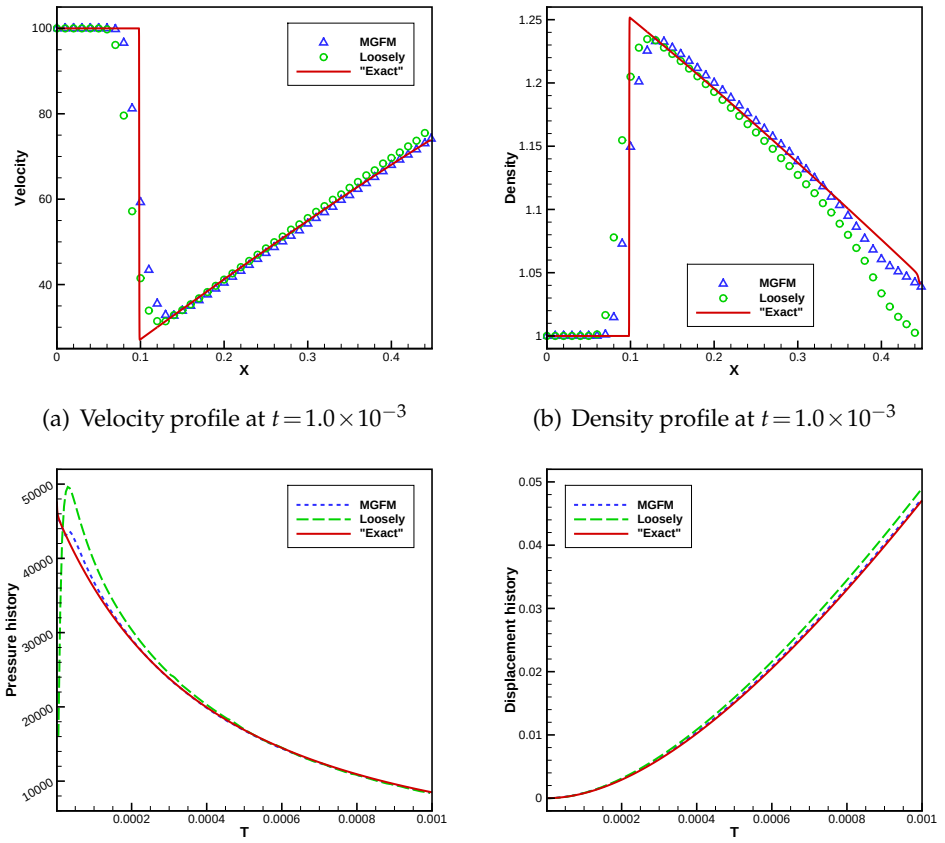

(a) Velocity profile at $t=1.0\times10^{-3}$

(b) Density profile at $t=1.0\times10^{-3}$

(c) Pressure history at the plate center

(d) Displacement history at the plate center

Figure 8: Case 4.2 A shock wave is generated in the water medium.

plate interaction problem with a relatively coarse mesh, where the space discretization is chosen as $\Delta x=1.0\times10^{-2}$ in the fluid domain. As shown in Fig. 8(a), the MGFM is a little better than the loosely-coupled method for simulating the velocity profile near the interface. It should be noted that the overheating phenomenon exists near the interface in Fig. 8(b), no matter what method is used. Comparatively speaking, it is suppressed well by the MGFM. Several curves in Fig. 8(c) depict the center pressure history. The loosely-coupled method is unable to faithfully take into account the simultaneous interaction between different media. This causes that the pressure curve starts from a very low point, and then rises rapidly. During this time period the pressure differs from the "exact solution" significantly. Then there is a pressure-drop process. During this time period the pressure trend concurs with the "exact solution", but there are still some discrepancies. On the contrary, the MGFM faithfully takes into account the simultaneous interaction occurring at the interface, which leads to a much better result during all the time periods. Fig. 8(d) depicts the center displacement history. In this figure, the center

displacement difference between the result by the loosely-coupled method and the "exact solution" becomes more and more visible as time progresses, but this phenomenon is not obvious for the MGFM.

Case 4.3 (Performance under extreme conditions)**.** Although these two method both work in the above cases, the loosely-coupled method is much worse than the MGFM on the accuracy. To better understand the superiority of the MGFM, an extreme and special example is designed and tested here. The loosely-coupled method, for this example, fails to provide a positive interfacial pressure, which directly leads to the failure of calculation. Nevertheless, the MGFM performs consistently. The material of the plate is chosen to be stainless steel, with some non-dimensional parameters like elastic modulus of 2.05×10^6, density of 7.8, Poisson's ratio of 0.3, side length of 10.0 and thickness of 0.2. The mesh used is $\Delta x=5.0\times10^{-3}$ in the fluid domain and also $\Delta\xi=0.5$ in the solid domain. The CFL number is specially set to be 1.0. This is a problem where a shock wave is generated in the air medium and can be work out by the loosely-coupled method, see Fig. 9. However, if all the conditions and parameters remain unaltered except that the density of the plate is replaced by $\rho_s=0.2$, the loosely-coupled method provides a solution with an obvious error at the location of the shock front, see Fig. 10. Even worse, "negative" pressure may be generated using this method. That is why we choose $t=4.27\times10^{-5}$ as the terminal time. Next time step the computation will collapse due to "negative" pressure. However, this problem does not exist with the MGFM, no matter how long the computation time is taken.

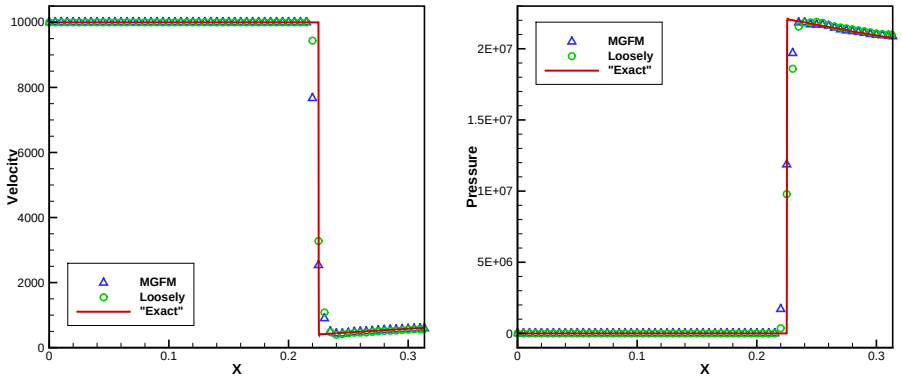

(a) Velocity profile at $t=4.27\times10^{-5}$ (b) Pressure profile at $t=4.27\times10^{-5}$

Figure 9: Case 4.3(a): The material of the plate is stainless steel.

Case 4.4 (Acceleration techniques)**.** In this case, we aim to validate and compare the different acceleration techniques in Subsection 3.4. The material of the plate and the initial conditions are chosen as those in Case 4.3. The space discretization is chosen as $\Delta x=5.0\times10^{-3}$ in the fluid domain and $\Delta\xi=5.0\times10^{-3}$ in the solid domain. In order to carry out a comparison, we take the result obtained with the fixed coupling time step

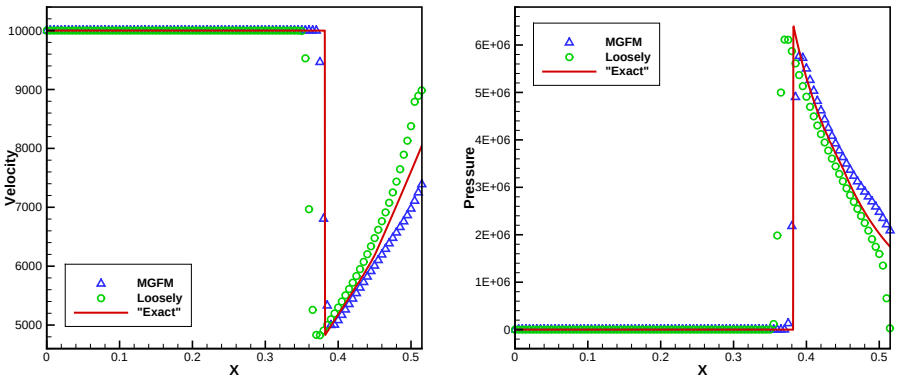

(a) Velocity profile at $t=4.27\times10^{-5}$ (b) Pressure profile at $t=4.27\times10^{-5}$

Figure 10: Case 4.3(b): The density of the plate is replaced by $\rho_s=0.2$.

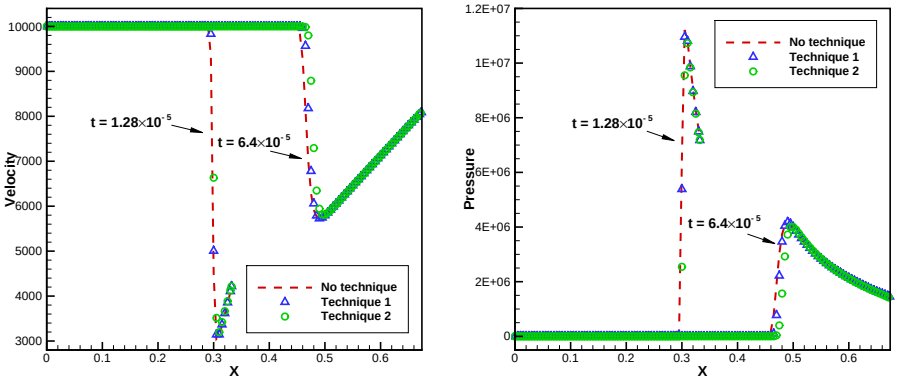

(a) Velocity profile (b) Pressure profile

Figure 11: Case 4.4: Comparison of different acceleration techniques.

$\Delta t=6.4\times10^{-8}$ as the numerical solution without any acceleration technique, because this time step satisfies both the conditions (3.8) and (3.9). In the meantime, we try to use Technique 1 and 2 for acceleration with a larger coupling time step, e.g., $\Delta t=3.2\times10^{-7}$, to solve the same problem. This time step satisfies (3.8) but does not satisfy (3.9). We divide one time step size into 5 sub-time intervals to calculate the plate deformation with condition (3.9) satisfied. A simple comparison at respective $t=1.28\times10^{-5}$ and $t=6.4\times10^{-5}$ is given in Fig. 11. Note that the results without any acceleration technique are obtained after 200 steps for $t=1.28\times10^{-5}$ and after 1000 steps for $t=6.4\times10^{-5}$. If one acceleration technique is applied, the time step numbers can be reduced to 40 and 200, respectively. There is no apparent difference for these two techniques in the velocity or pressure profile, see Figs. 11(a) and 11(b). We primarily apply Technique 2 into our following computations for its easy implementation. Further validation for Technique 2 is given in the two-dimensional UNDEX examples.

5 Numerical experiments and discussions

In the following, a series of simulations of UNDEX near an elastic plate consists of the generation and propagation of blast wave and the response of structure. Physically, rapid changes of pressure may cause the formation of cavitation in the fluid at the fluid-plate interface because the fluid usually can not withstand tension. The appearance of cavitation imposes difficulties in the treatment of the interface. Up to present, there is no well-developed numerical technique to treat the cavitation-structure interaction. Only attempts have been made for Euler-Euler coupling [20]. We, therefore, only consider the dynamic process of plate structure under the impact of shock waves until the incipience of cavitation. Some examples are given below.

5.1 A case of UNDEX

In the following calculations, we assume that there is a square plate with two opposite edges clamped on the water surface, and a cylindrical explosive source beneath it. See Fig. 12(a). Flow fields or deformations of plate at all cross-sections of this three-dimensional model are identical. This simulation, therefore, can be simplified to a two-dimensional model. The thin plate is initially located at the straight line $y=2$m with thickness of 0.25m. This plate is set to be a stainless steel plate and its material properties are $E_s=2.05\times10^{11}$Pa, $\nu=0.3$, $\rho_s=7800\text{kg/m}^3$. The initial real computational domain for fluid is a rectangular region with $\text{X}\times\text{Y}\in[-5\text{m},5\text{m}]\times[-5\text{m},2\text{m}]$. The deformation of structure under impact loading will cause a small geometry change of computational domain. So we should reserve a little computational space beyond $y=2$m. An explosive gas bubble with a radius of 0.5m is located at the origin $(0.0,0.0)$ in water. See Fig. 12(b). The initial conditions for these two fluids are shown in Table 2. A total of 321×225 uniform grid points are distributed in the real fluid computational domain, and 21×21 uniform grid points are distributed in the plate computational domain. The CFL number is set to 0.45. The nonreflective boundary conditions are used for all the fluid outside boundaries. The gas bubble-water coupling is treated as the original MGFM in [12]. To capture the moving gas-water interface, the level set technique is utilized.

In order to clearly demonstrate the evolution of strong shock impacting on the thin plate and the dynamic response of the thin plate, the pressure contours at different stages of earlier times are shown in Fig. 13. The dashed circle represents the initial bubble while the solid circle represents the expanded bubble. Fig. 13(a) shows that once the explosion starts, a strong underwater shock is generated and propagates radially outwards with decreasing strength. Fig. 13(b) shows that the underwater shock soon impacts the

Table 2: Initial conditions of explosive bubble and water.

Medium	u (m/s)	v (m/s)	ρ (kg/m^3)	p (Pa)
Bubble	0.0	0.0	1270.0	8.29×10^8
Water	0.0	0.0	1000.0	1.0×10^5

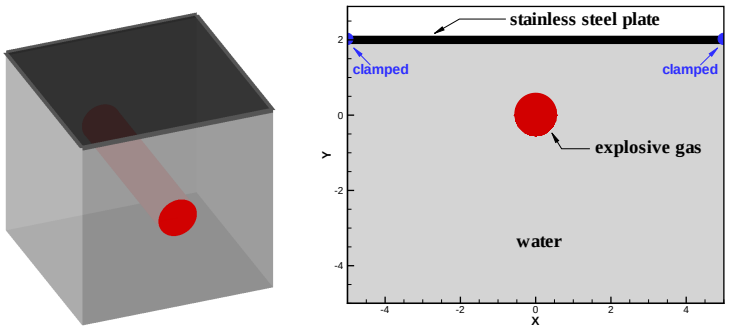

(a) 3D illustration (b) 2D illustration

Figure 12: Schematic diagram for UNDEX near a thin elastic plate.

plate, resulting in the incident shock reflected from the fluid-plate interface. The reflection wave with a decreasing strength travels towards the expanding explosion bubble surface. A tiny deformation in the normal direction of the plate surface is formed, but it is not easy to observe the change at this stage. Fig. 13(c) shows that the reflected wave, as a result of contacting the expanded bubble, is divided into two parts: one is transmitted into the air bubble, while the other is reflected as a rarefaction wave propagating along the opposite direction. After the reflected rarefaction wave reaches the bottom surface of the plate, the wave-plate interaction causes a low pressure region formed. As time goes on, the pressure there keeps on decreasing such that the pressure in the low pressure region drops below saturated pressure, leading to the incipience of cavitation. See Fig. 13(d). The thin plate, under the lasting impact of load, has presented a certain degree of bending. Because the material used is steel with larger elastic modulus, the deformation rate is relatively small.

Fig. 14 records the pressure history at the plate center for three structure mesh sizes. A large pressure peak can be found in this figure, which is generated by underwater shock impact. The peak lasts for a short time, and decays rapidly. A low-pressure period is then formed, which can be regarded due to the formation and evolution of cavitation. The number of real fluid grid points is fixed as 321×225, and the number of structure grid points is taken as 11×11, 21×21 and 81×81, respectively. It is worth mentioning that a finer mesh for the flow field is required to produce a good numerical resolution, while this is not needed for the plate calculation due to the regular geometry and the feature of small deformation. As shown in Fig. 14, there is no obvious difference among these three test meshes. In the following, the fluid and structure grid points are still taken to be 321×225 and 21×21, respectively.

To further validate the second acceleration technique (Technique 2) in Subsection 3.4, Fig. 15 provides us a simple comparison of the fluid-plate interface displacement and velocity profiles at $t=1.0$ms, 1.7ms and 2.4ms. We divide one time step size into 100 sub-time intervals to calculate the plate deformation for comparison purposes. There is no significant difference between the two measures, as shown in Fig. 15.

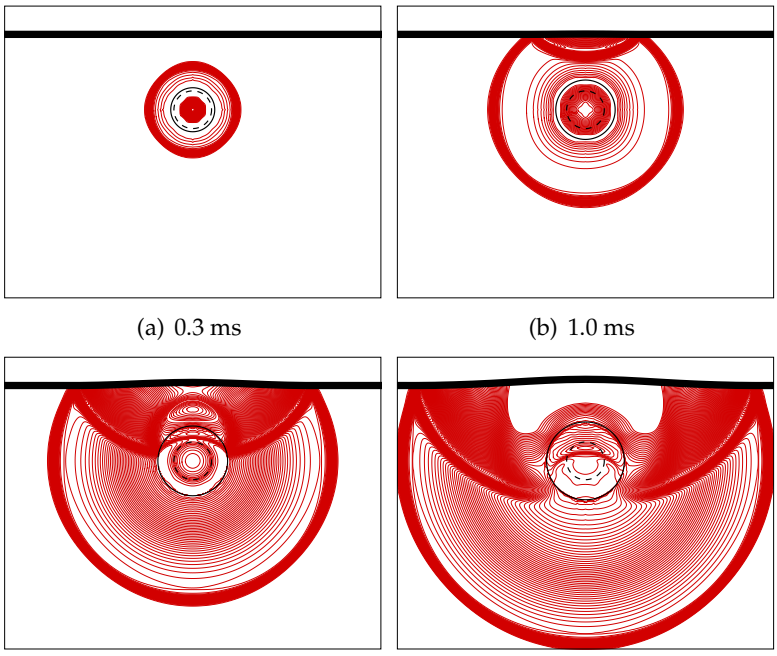

(a) 0.3 ms (b) 1.0 ms

(c) 1.7 ms (d) 2.4 ms

Figure 13: Pressure contours at different times.

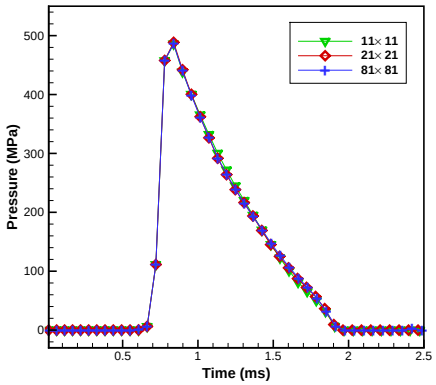

Figure 14: Comparison of pressure history at the plate center for different solid grid points.

5.2 Influence of structure flexibility on the flow field

Numerical tests show that the MGFM, because of taking into account the nonlinear fluid-plate interaction, can provide accurate interfacial states. To better observe the effect of structure flexibility on interaction occurring at the interface, we construct and simulate a set of UNDEX problems in conjunction with some purpose-designed thin elastic plates. Without loss of generality, the material property parameters are fixed by $\nu = 0.3$, $\rho_s = 5000\text{kg}/\text{m}^3$ except E_s is constantly adjusted from $E_s = 1.0\times10^{11}$Pa to $E_s = 1.0\times10^{21}$Pa. For

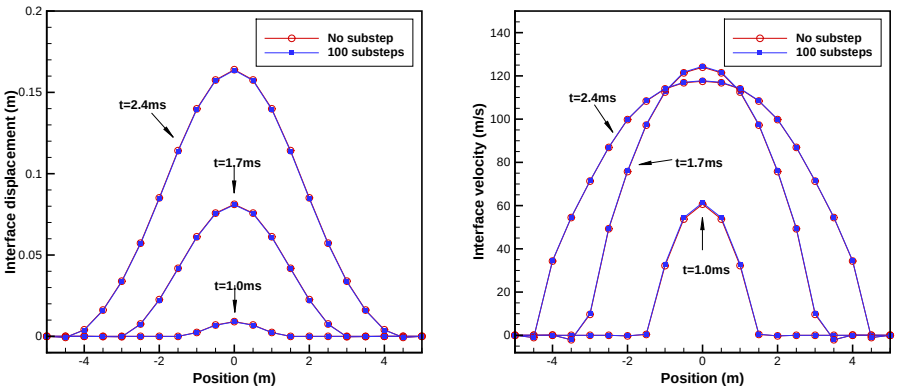

(a) Interface displacement profile (b) Interface velocity profile

Figure 15: Comparison of interface status at different times.

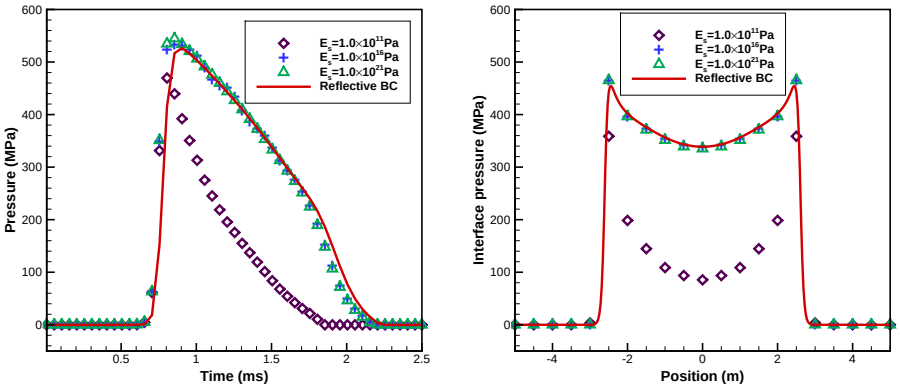

(a) Pressure history at the plate center (b) Interface pressure at $t=1.5$ms

Figure 16: Comparison among different elastic moduli.

a large elastic modulus, too much simulation time is needed for a general FSI procedure and this may be unendurable. But with the employment of Technique 2 for acceleration in Subsection 3.4, MGFM is capable of efficiently simulating the processes of UNDEX for different structural flexibilities. Figs. 16(a) and 16(b) respectively record the center pressure history and interface pressure distribution at $t=1.5$ms under three types of elastic moduli and reflective boundary condition. A comparison shows that the structure flexibility affects the shock impact significantly and a more flexible material causes the cavitation to occur earlier. It is more obviously if the elastic modulus is relatively small, say, $E_s=1.0\times10^{11}$Pa. It is also found that the result, if the plate rigidity is large enough, concurs well with that under the reflective boundary condition by assuming the plate is rigid.

The flow fields (pressure) at $t=2.0$ms among different elastic moduli and reflective boundary condition are presented in Fig. 17. Due to symmetry, only half of the computa-

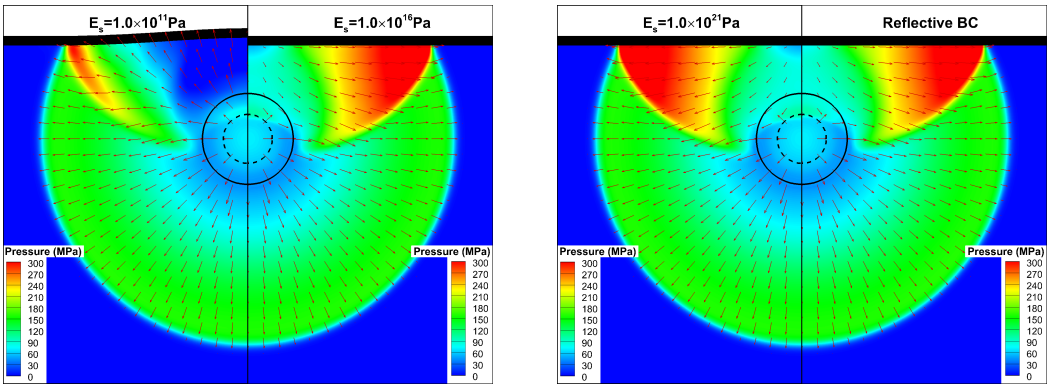

(a) $E_s=1.0\times10^{11}$Pa and $E_s=1.0\times10^{16}$Pa

(b) $E_s=1.0\times10^{21}$Pa and reflective boundary condition

Figure 17: Comparison of the flow fields among different elastic moduli and reflective boundary condition at $t=2.0$ms.

tional domain is plotted. The vectors correspond to the fluid velocity. As the plate bends, it expands the fluid region below the material surface, leading to reducing the shock strength. A cavitation region where the pressure is near zero can be found on the left side of Fig. 17(a), while this phenomenon does not exist on the right side of Fig. 17(a). Generally speaking, the plate with smaller elastic modulus leads to weaker interface pressure due to lower material rigidity. Also, the curvature of the two plates is not the same due to the different interface loading and rigidity. The plate on the left side features larger interface displacement. Fig. 17(b) shows that the fluid and plate response remains almost the same between $E_s=1.0\times10^{21}$Pa and reflective boundary condition. This is consistent with the actual physical situation, because the plate with an extremely large elastic modulus could be considered similar to a rigid plate.

6 Conclusions

In this work, the MGFM originally applied to treat multi-fluid coupling was extended to treat flow and thin plate nonlinear interaction. By solving shock relationship and thin-elastic-plate equation together to predict the ghost fluid states and the plate loading, this approach not only ensured numerical stability and maintained the advantages of simplicity and high efficiency, but also provided a more accurate interface boundary condition. In addition, there were no irregular grid cells required for special treatment due to the definition of ghost cells and ghost fluids. An acceleration technique of the coupling process was also implemented for improving efficiency. Multiple numerical experiments were presented and analyzed to show that this method was capable of providing correct results with robust and consistent performance, especially in case the interaction between the fluid and the structure is very strong. The evolution of strong shock impacting on the thin plate and dynamic response of the thin plate subjected to UNDEX was systematically

investigated.

The present technique of treating the fluid-structure coupling relies on the assumption that the solid is a rectangular plate, and we believe that the MGFM can be made to work for other thin plates or shell structures for a long-time simulation with fluid phase transition or cavitation involved. These are our future works.

Appendix: Difference discretization scheme of (2.7)

Each partial derivative term at the interior grid point (ξ_i,η_j) and time t^n in (2.7) can be approximated by a difference equation as follows:

$$\left(\frac{\partial^4 w}{\partial\xi^4}\right)^n_{i,j}=\frac{1}{\Delta\xi^4}\left(w^n_{i+2,j}-4w^n_{i+1,j}+6w^n_{i,j}-4w^n_{i-1,j}+w^n_{i-2,j}\right), \tag{A.1a}$$

$$\left(\frac{\partial^4 w}{\partial\eta^4}\right)^n_{i,j}=\frac{1}{\Delta\eta^4}\left(w^n_{i,j+2}-4w^n_{i,j+1}+6w^n_{i,j}-4w^n_{i,j-1}+w^n_{i,j-2}\right), \tag{A.1b}$$

$$\begin{aligned}\left(\frac{\partial^4 w}{\partial\xi^2\partial\eta^2}\right)^n_{i,j}=\frac{1}{\Delta\xi^2\Delta\eta^2}\Big(&4w^n_{i,j}-2\left(w^n_{i+1,j}+w^n_{i,j-1}+w^n_{i-1,j}+w^n_{i,j+1}\right)\\&+w^n_{i+1,j+1}+w^n_{i+1,j-1}+w^n_{i-1,j-1}+w^n_{i-1,j+1}\Big),\end{aligned} \tag{A.1c}$$

$$\left(\frac{\partial^2 w}{\partial t^2}\right)^n_{i,j}=\frac{w^{n+1}_{i,j}-2w^n_{i,j}+w^{n-1}_{i,j}}{\Delta t^2}. \tag{A.1d}$$

Direct substitution of (A.1a)-(A.1d) into (2.7) gives

$$w^{n+1}_{i,j}=\frac{\Delta t^2}{\rho_s h}\left(q^n_{i,j}-D\nabla^2_h\nabla^2_h w^n_{i,j}\right)+2w^n_{i,j}-w^{n-1}_{i,j}, \tag{A.2}$$

where

$$\begin{aligned}\nabla^2_h\nabla^2_h w^n_{i,j}=&\widetilde{A}w^n_{i,j}+\widetilde{B}\left(w^n_{i+1,j}+w^n_{i-1,j}\right)+\widetilde{C}\left(w^n_{i,j+1}+w^n_{i,j-1}\right)+\widetilde{D}\left(w^n_{i+2,j}+w^n_{i-2,j}\right)\\&+\widetilde{E}\left(w^n_{i,j+2}+w^n_{i,j-2}\right)+\widetilde{F}\left(w^n_{i+1,j+1}+w^n_{i+1,j-1}+w^n_{i-1,j-1}+w^n_{i-1,j+1}\right),\end{aligned}$$

and

$$\widetilde{A}=\frac{6}{\Delta\xi^4}+\frac{6}{\Delta\eta^4}+\frac{8}{\Delta\xi^2\Delta\eta^2},\qquad \widetilde{B}=-\frac{4}{\Delta\xi^4}-\frac{4}{\Delta\xi^2\Delta\eta^2},\qquad \widetilde{C}=-\frac{4}{\Delta\eta^4}-\frac{4}{\Delta\xi^2\Delta\eta^2},$$

$$\widetilde{D}=\frac{1}{\Delta\xi^4},\qquad \widetilde{E}=\frac{1}{\Delta\eta^4},\qquad \widetilde{F}=\frac{2}{\Delta\xi^2\Delta\eta^2}.$$

The difference schemes for the boundary conditions (2.8) and (2.9), for example at $\xi=\xi_0$, $\xi=\xi_{-1}$, can be respectively written as

$$w^n_{0,j}=0 \quad\text{and}\quad w^n_{-1,j}=3w^n_{1,j}-0.5w^n_{2,j}, \tag{A.3a}$$

$$w^n_{0,j}=0 \quad\text{and}\quad w^n_{-1,j}=-w^n_{1,j}. \tag{A.3b}$$

Acknowledgments

The authors would like to thank the referees for valuable comments and suggestions. This work is supported under the National Natural Science Foundation of China (Nos. 11201442 and 10931004).

References

[1] B. COCKBURN, S. Y. LIN AND C. W. SHU, *TVB Runge-Kutta local projection discontinuous Galerkin finite element method for conservation laws III: one dimensional systems*, J. Comput. Phys., 84 (1989), pp. 90–113.

[2] B. COCKBURN, S. HOU AND C. W. SHU, *The Runge-Kutta local projection discontinuous Galerkin finite element method for conservation laws IV: the multidimensional case*, Math. Comput., 54 (1990), pp. 545–581.

[3] A. HARTEN AND S. OSHER, *Uniformly high-order accurate nonoscillatory schemes I*, SIAM J. Numer. Anal., 24 (1987), pp. 279–309.

[4] G. S. JIANG AND C. W. SHU, *Efficient implementation of weighted ENO schemes*, J. Comput. Phys., 126 (1996), pp. 202–228.

[5] R. K. JAIMAN, X. JIAO, P. H. GEUBELLE AND E. LOTH, *Conservative load transfer along curved fluid-solid interface with non-matching meshes*, J. Comput. Phys., 218 (2006), pp. 372–397.

[6] C. FARHAT, K. G. VAN DER ZEE AND P. GEUZAINE, *Provably second-order time-accurate loosely-coupled solution algorithms for transient nonlinear computational aeroelasticity*, Comput. Methods Appl. Mech. Eng., 195 (2006), pp. 1973–2001.

[7] A. V. ZUIJLEN, A. D. BOER AND H. BIJL, *Higher-order time integration through smooth mesh deformation for 3D fluid-structure interaction simulations*, J. Comput. Phys., 224 (2007), pp. 414–430.

[8] R. JAIMAN, P. GEUBELLE, E. LOTH AND X. JIAO, *Combined interface boundary condition method for unsteady fluid-structure interaction*, Comput. Methods Appl. Mech. Eng., 200 (2011), pp. 27–39.

[9] T. NAKATA AND H. LIU, *A fluid-structure interaction model of insect flight with flexible wings*, J. Comput. Phys., 231 (2012), pp. 1822–1847.

[10] R. P. FEDKIW, T. ASLAM, B. MERRIMAN AND S. OSHER, *A non-oscillatory Eulerian approach to interfaces in multimaterial flows (the ghost fluid method)*, J. Comput. Phys., 152 (1999), pp. 457–492.

[11] R. P. FEDKIW, *Coupling an Eulerian fluid calculation to a Lagrangian solid calculation with the ghost fluid method*, J. Comput. Phys., 175 (2002), pp. 200–224.

[12] T. G. LIU, B. C. KHOO AND K. S. YEO, *Ghost fluid method for strong shock impacting on material interface*, J. Comput. Phys., 190 (2003), pp. 651–681.

[13] T. G. LIU, B. C. KHOO AND C. W. WANG, *The ghost fluid method for compressible gas-water simulation*, J. Comput. Phys., 204 (2005), pp. 193–221.

[14] C. W. WANG, T. G. LIU AND B. C. KHOO, *A real-ghost fluid method for the simulation of multimedium compressible flow*, SIAM J. Sci. Comput., 28 (2006), pp. 278–302.

[15] J. X. QIU, T. G. LIU AND B. C. KHOO, *Simulations of compressible two-medium flow by Runge-Kutta discontinuous Galerkin methods with the ghost fluid method*, Commun. Comput. Phys., 3 (2008), pp. 479–504.

[16] C. W. WANG, H. Z. TANG AND T. G. LIU, *An adaptive ghost fluid finite volume method for compressible gas-water simulations*, J. Comput. Phys., 227 (2008), pp. 6385–6409.
[17] P. T. BARTON AND D. DRIKAKIS, *An Eulerian method for multi-component problems in non-linear elasticity with sliding interfaces*, J. Comput. Phys., 229 (2010), pp. 5518–5540.
[18] L. XU AND T. G. LIU, *Optimal error estimation of the modified ghost fluid method*, Commun. Comput. Phys., 8 (2010), pp. 403–426.
[19] L. XU AND T. G. LIU, *Accuracies and conservation errors of various ghost fluid methods for multi-medium Riemann problem*, J. Comput. Phys., 230 (2011), pp. 4975–4990.
[20] T. G. LIU, B. C. KHOO AND W. F. XIE, *The modified ghost fluid method as applied to extreme fluid-structure interaction in the presence of cavitation*, Commun. Comput. Phys., 1 (2006), pp. 898–919.
[21] W. F. XIE, Y. L. YOUNG, T. G. LIU AND B. C. KHOO, *Dynamic response of deformable structures subjected to shock load and cavitation reload*, Comput. Mech., 40 (2007), pp. 667–681.
[22] T. G. LIU, W. F. XIE AND B. C. KHOO, *The modified ghost fluid method for coupling of fluid and structure constituted with hydro-elasto-plastic equation of state*, SIAM J. Sci. Comput., 30 (2008), pp. 1105–1130.
[23] W. F. XIE, Y. L. YOUNG AND T. G. LIU, *Multiphase modeling of dynamic fluid-structure interaction during close-in explosion*, Int. J. Numer. Meth. Eng., 74 (2008), pp. 1019–1043.
[24] H. S. TANG AND F. SOTIROPOULOS, *A second-order Godunov method for wave problems in coupled solid-watergas systems*, J. Comput. Phys., 151 (1999), pp. 790–815.
[25] T. G. LIU, J. Y. HO, B. C. KHOO AND A. W. CHOWDHURY, *Numerical simulation of fluid-structure interaction using modified ghost fluid method and Naviers equations*, J. Sci. Comput., 36 (2008), pp. 45–68.
[26] T. G. LIU, A. W. CHOWDHURY AND B. C. KHOO, *The modified ghost fluid method applied to fluid-elastic structure interaction*, Adv. Appl. Math. Mech., 3 (2011), pp. 611–632.
[27] W. F. XIE, Z. K. LIU AND Y. L. YOUNG, *Application of a coupled Eulerian-Lagrangian method to simulate interactions between deformable composite structures and compressible multiphase flow*, Int. J. Numer. Meth. Eng., 80 (2009), pp. 1497–1519.
[28] Y. L. YOUNG, Z. K. LIU AND W. F. XIE, *Fluid-structure and shock-bubble interaction effects during underwater explosions near composite structures*, ASME J. Appl. Mech., 76 (2009), 051303.
[29] Z. K. LIU, W. F. XIE AND Y. L. YOUNG, *Numerical modeling of complex interactions between underwater shocks and composite structures*, Comput. Mech., 43 (2009), pp. 239–251.
[30] Z. K. LIU, W. F. XIE AND Y. L. YOUNG, *Transient response of partially-bonded sandwich plates subject to underwater explosions*, Shock Vib., 17 (2010), pp. 233–250.
[31] B. VAN LEER, *Towards the ultimate conservative difference scheme IV: a new approach to numerical convection*, J. Comput. Phys., 23 (1977), pp. 276–299.
[32] A. HARTEN, P. D. LAX AND B. VAN LEER, *On upstream differencing and Godunov-type schemes for hyperbolic conservation laws*, SIAM Rev., 25 (1983), pp. 35–61.
[33] T. G. LIU, B. C. KHOO AND K. S. YEO, *The simulation of compressible multi-medium flow, Part I: a new methodology with test applications to 1D gas-gas and gas-water cases*, Comput. Fluids, 30 (2001), pp. 291–314.
[34] M. SUSSMAN, P. SMEREKA AND S. OSHER, *A level set approach for computing solutions to incompressible two-phase flow*, J. Comput. Phys., 114 (1994), pp. 146–159.
[35] S. O. UNVERDI AND G. TRYGGVASON, *A front-tracking method for viscous incompressible multi-fluid flows*, J. Comput. Phys., 100 (1992), pp. 25–37.
[36] S. TIMOSHENKO AND S. WOINOWSKY-KRIEGER, Theory of Plates and Shells, Second ed., McGraw Hill, 1959.